

# Solar eruptions: the CME-flare relationship

B. Vršnak\*

Hvar Observatory, Faculty of Geodesy, University of Zagreb, Kačićeva 26, HR-10000 Zagreb, Croatia

Received XXXX, accepted XXXX

Published online XXXX

**Key words** Sun: coronal mass ejections (CMEs) – Sun: flares

Coronal mass ejections (CMEs), caused by large-scale eruptions of the coronal magnetic field, often are accompanied by a more localized energy release in the form of flares, as a result of dissipative magnetic-field reconfiguration. Morphology and evolution of such flares, also denoted as dynamical flares are often explained as a consequence of reconnection of the arcade magnetic field, taking place below the erupting magnetic flux rope. A close relationship of the CME acceleration and the flare energy release is evidenced by various statistical correlations between parameters describing CMEs and flares, as well as by the synchronization of the CME acceleration phase with the impulsive phase of the associated flare. Such behavior implies that there must be a feedback relation between the dynamics of the CME and the flare-associated reconnection process. From the theoretical standpoint, magnetic reconnection affects the CME dynamics in several ways. First, it reduces the tension of the overlying arcade magnetic field and increases the magnetic pressure below the flux rope, and in this way enhances the CME acceleration. Furthermore, it supplies the poloidal magnetic flux to the flux rope, which helps sustaining the electric current in the rope and prolonging the action of the driving Lorentz force to large distances. The role of these processes, directly relating solar flares and CMEs, is illustrated by employing a simple model, where the erupting structure is represented by a curved flux rope anchored at both sides in the dense/inert photosphere, being subject to the kink and torus instability. It is shown that in most strongly accelerated ejections, where values on the order of  $10 \text{ km s}^{-2}$  are attained, the poloidal flux supplied to the erupting rope has to be several times larger than was the initial flux.

Copyright line will be provided by the publisher

## 1 Introduction

Solar flares are frequently accompanied by explosive eruptions of the coronal magnetic structures that take a form of the so-called coronal mass ejections (CMEs). In such eruptive events these two phenomena are tightly related, indicating that they are a consequence of a common underlying process (for a discussion see, e.g., Švestka 2001, and references therein). Bearing in mind that non-thermal and thermal energy release in flares is obviously governed by dissipative/resistive processes, whereas the eruptions themselves are apparently caused by ideal MHD processes, the tight relationship of flare and CME processes indicates that there is a feedback relationship (Temmer et al. 2010) between the processes that occur at plasma micro-scales and MHD processes that develop on the active-region scales and expand up to global scales.

The flare-CME relationship is most clearly seen in the so called two-ribbon flares, sometimes also called dynamical flares or solar storms (for terminology and historical aspects see, e.g., Priest 1982; Švestka 1976, 2001). This type of flare/ejection relationship is known already from the times when only  $H\alpha$  observations were available for studies of eruptive events. Two-ribbon flares are called so due to the occurrence of two flare ribbons laterally expand-

ing away from the polarity inversion line (PIL). Usually such events start by a slow rise and swelling of the PIL filament. At a certain moment, the filament erupts and the flare ribbons occur. After the flare impulsive phase, usually marked by occurrence of radio type III bursts, fast rise of soft X-ray (SXR) flux, microwave and hard X-ray (HXR) burst, a growing system of hot flare loops appears, gradually shrinking and cooling to chromospheric temperatures (e.g., Švestka 1987; Veronig et al. 2006; Vršnak et al. 2006, and reference therein). Such a behavior led to a two-dimensional (2D) phenomenological concept of two-ribbon flares, frequently called a CSHKP model (Carmichael 1964; Hirayama 1974; Kopp & Pneuman 1976; Sturrock 1966), which explains most of the morphological characteristics of such events, as well as synchronization of the eruption and flare energy release by introducing a concept of magnetic reconnection below the erupting flux rope.

The aim of this paper is to review observational and theoretical aspects of the flare-CME relationship, paying special attention to basic physical concepts that govern this relationship (for other recent reviews see, e.g., Aulanier 2014; Schmieder et al. 2015, and references therein). In particular, we illustrate how, and to a what degree magnetic reconnection (i.e., the resistive process) affects the ideal processes (e.g., kink or torus instability) that drive the eruption, as well as how it influences the acceleration and propagation

\* Corresponding author: bvršnak@geof.hr

of the flare-associated CME. In Section 2 we present the empirical aspect of the relationship. In Section 3 a simple flux-rope model is employed to explain the observations. The outcome is summarized and discussed in Section 4.

## 2 Observational aspects

Although flares and CMEs are characterized by a broad variety of morphological, evolutionary, and kinematical characteristics, there are some common properties observed in most events. Eruptions most often show accelerations on the order of  $100 \text{ m s}^{-2}$  (e.g., Bein et al. 2011; Vršnak et al. 2007; Zhang & Dere 2006), but the most powerful events can attain accelerations on the order of  $10 \text{ km s}^{-2}$  (e.g., Bein et al. 2011; Vršnak et al. 2007; Williams et al. 2005). Maximum velocities range from several tens  $\text{km s}^{-1}$ , up to more than  $2000 \text{ km s}^{-1}$  (Yashiro et al. 2004). Statistically speaking, more powerful CMEs are accompanied by more powerful flares (e.g., Bein et al. 2012; Burkepile et al. 2004; Moon et al. 2003, 2002; Vršnak et al. 2005), representing one of the most basic statistical evidences of the common physical background of these two types of events.

As a matter of fact, it was shown by Vršnak et al. (2005) and more recently by Bein et al. (2012) that, generally, there is a hierarchy of events related to their flare association: Eruptions launched from spotless regions that are not associated with any significant flare signature are characterized by the weakest accelerations, but the accelerations are still comparable to those found in active-region CMEs associated with weak flares of SXR-class A, B and C. On the other hand, eruptions associated with flares of SXR-class M and X show significantly stronger accelerations. However, this cannot be taken as an evidence for two *distinct* classes of CMEs (flare/non-flare), as proposed by Gosling et al. (1976) and MacQueen & Fisher (1983), which became a widely accepted concept that was frequently used to interpret various aspects of CMEs (see, e.g., Andrews & Howard 2001; Low & Zhang 2002; Moon et al. 2002; Sheeley et al. 1999). On the contrary, it is an evidence that there is a “continuum” of events from weak to strong ones, the ejection acceleration increasing with the increasing importance of the associated flares. It should be also stressed that although the eruptions accompanied by filament ejections on average have significantly lower accelerations, their maximum speeds are on average only marginally lower than that of flare-associated CMEs (Vršnak et al. 2005). This evidences that a filament (i.e., a dense/heavy prominence) increases the inertia of the structure, causing a more gradual ejection in the initial phase, but does not prohibit it to reach high velocities if the acceleration lasts long enough, i.e., the physical background is more or less the same as in eruptions not including a filament.

Another essential observational aspect is synchronization of the rising phase of the SXR burst and the acceleration phase of the ejection, reported by, e.g., Kahler et al. (1988); Maričić et al. (2004); Neupert et al. (2001); Shanmugaraju

et al. (2003); Vršnak et al. (2004); Zhang & Dere (2006); Zhang et al. (2001, 2004)). Following these case-studies, Maričić et al. (2007) and Bein et al. (2012) applied a statistical approach, undoubtedly confirming that such a synchronization exists in the majority of studied dynamical flares. The main outcome of these two studies was that the ejection acceleration peaks very close to the peak of the derivative of the flare-associated SXR flux. However, it should be emphasized that Maričić et al. (2007) recognized that about one quarter of analyzed events does not show such a behavior, and furthermore, even in “synchronized events”, in majority of cases the CME acceleration starts *before* the SXR burst, and ends *after* it reaches maximum. This outcome was confirmed later on by Bein et al. (2012).

The described overall synchronization indicates that the ejection acceleration phase is related to the flare impulsive phase, since the SXR burst rise is usually considered to be a cumulative consequence of the flare non-thermal energy release that is revealed by the associated HXR and microwave burst (so-called “Neupert effect”; Neupert (1968); see also Dennis & Zarro (1993); Veronig et al. (2002) and references therein). Indeed, recent studies presented by Temmer et al. (2008) and Temmer et al. (2010) have demonstrated clearly that the ejection acceleration phase is very closely related to the flare-associated HXR burst, representing the most direct evidence of the synchronization of the ejection acceleration phase and the flare impulsive phase. In this respect it should be stressed that detailed inspection of graphs presented in these two studies again discloses that the acceleration starts before the flare impulsive phase, represented now directly by the HXR burst, and ends after it. Finally, Berkebile-Stoiser et al. (2012) showed that the hardness of the flare HXR spectra is distinctly correlated with the CME acceleration. In most of the events, the CME acceleration started before the flare. In addition, from the time difference between flare and CME start, it was inferred that the current sheet length at the onset of magnetic reconnection is of the order of 20 Mm.

Bearing in mind that the flare energy release rate is related to the magnetic reconnection rate (see, e.g., Miklenic et al. 2009, 2007), the presented arguments indicate that in most events there is a feedback relationship connecting the ejection dynamics and the flare-related reconnection process below the erupting flux rope – enhanced reconnection rate increases the ejection acceleration and on the other hand, enhanced acceleration provides more powerful reconnection (for details see Temmer et al. 2010; Vršnak 2008). Such a hypothesis is strongly supported by the outcome of the studies presented by Qiu & Yurchyshyn (2005) and Miklenic et al. (2009), where it was demonstrated that the ejection velocity and the SXR flare importance are closely correlated with the reconnected flux. However, the strongest evidence is provided by the case studies by Qiu et al. (2004) and Wang et al. (2003), where it was revealed that the eruptive prominence acceleration was tightly synchronized with

the reconnection rate (so-called “flux change rate”) in the associated two-ribbon flare.

An important aspect of the timing analyzes is that the eruption in the majority of events starts earlier than the two-ribbon flare energy release (Bein et al. 2012; Maričić et al. 2007), evidencing that most often flares occur as a consequence of the eruption. Since signatures of dissipative processes (particle acceleration and Joule heating) are usually absent or are very weak in early phases of the eruption, it can be presumed that ejections are generally initiated by some ideal MHD process. The resistive processes, i.e., magnetic reconnection, start only after the rising flux rope achieves a certain height, giving enough space for the current sheet formation and an efficient reconnection process (see, e.g., Vršnak et al. 2003). Yet, in some events the flare energy release precedes the eruption (Bein et al. 2012; Maričić et al. 2007). This could be explained by occurrence of various forms of pre-eruptive magnetic field restructuring, leading to loss of equilibrium and the onset of eruptive instability. For instance, a confined flare can form a kink- or torus-unstable structure, which erupts immediately after being formed (e.g., Aurass et al. 1999). Analogously, a tether-cutting type of reconnection (Moore et al. 2001), or break-out reconnection (Antiochos 1998), might lead to the stage when the structure becomes unstable and erupts, resulting in a CME and the two-ribbon flare. Finally, it is possible that in some events the reconnection below the flux rope start before the eruption onset, increasing the electric current flowing along the flux rope and driving gradual evolution of the system to the loss of equilibrium and eruption (Vršnak 1990, 2008).

### 3 Theoretical aspects

#### 3.1 Basic physical concepts and constraints

As already mentioned, a dynamical-flare eruption is typically preceded by gradual evolution of the coronal magnetic structure through a series of quasi-equilibrium states, which can be driven by, e.g., converging motions and flux cancellation, shearing or twisting motions, emerging flux, gradual “tether-cutting” reconnection, etc. (e.g., Schmieder et al. 2015, and references therein). The pre-eruptive metastable structure evolves slowly until it loses equilibrium, when presumably an ideal MHD instability (e.g., kink or torus instability) sets-in and triggers the eruption. Such a scenario was studied by a number of authors, most often considering a flux-rope embedded in a coronal arcade, with footpoints anchored in the dense photosphere (see, e.g., Anzer 1978; Anzer & Pneuman 1982; Chen 1989; Gold & Hoyle 1960; Mouschovias & Poland 1978; Pneuman 1980; Sakurai 1976; Titov & Démoulin 1999; Török & Kliem 2003; van Tend 1979; Vršnak 1990).

Stability of such a system is determined by a number of parameters, most notably by the twist of the magnetic field lines, i.e., electric current  $I$  that flows along the flux rope

(see, e.g., Török & Kliem 2003; Vršnak 1990). Note that the stronger the current, the larger the amount of magnetic free energy stored in the system – in the simplest terms, the free energy can be expressed as  $W = LI^2$ , where  $L$  is the self-inductance of the system (for details see, e.g., Chen 1989; Garren & Chen 1994; Vršnak 2008; Žic et al. 2007). Thus, flux ropes carrying stronger currents are expected to erupt more violently.

This was clearly demonstrated by, e.g., Vršnak (1990), who studied stability and dynamics of a semi-toroidal flux rope anchored at both footpoints in the dense photosphere. In this analytical model a diamagnetic effect of the conductive photospheric surface (Kuperus & Raadu 1974) was included, which provided physical comprehension of a number of observational phenomena. For instance, the model is able to explain gradual transition of the system from a completely stable state to metastable state by, e.g., an increase of twist or longitudinal current (see Figure 5a of Vršnak 2008). The structure is in a metastable equilibrium at a given height that gradually increases as the current increases, which corresponds to the usually observed slow rise of the pre-eruptive structure. Furthermore, an unstable-equilibrium point at larger heights occurs, as shown in Figure 5a of Vršnak (2008). In such a situation, a small displacement from the metastable equilibrium results in oscillations, which explains, e.g., transversal prominence/filament oscillations (e.g., Ramsey & Smith 1966; Vršnak 1984). On the other hand, if the perturbation is strong enough, and the structure is moved from the metastable-equilibrium height to the unstable-equilibrium position, the structure erupts. This explains eruptions initiated by disturbance coming from a distant source (e.g., a large amplitude wave from another eruption).

Furthermore, for a certain domain in the parameter space, there is another stable-equilibrium point above both the metastable and the unstable equilibrium position (see Figure 5b of Vršnak 2008). This explains oscillations sometimes observed after failed eruptions (e.g., Vršnak et al. 1990). Finally, a persistent gradual change of model parameters (e.g., increasing twist and/or current, or decreasing mass, etc.) eventually leads to a loss of equilibrium, approximately at a height comparable to flux-rope footpoint half-distance. In other words, the structure evolves through a series of quasi-equilibrium states until it comes to a position where there is no neighboring static equilibrium available, so the structure has to respond dynamically, i.e., it erupts. One of direct successes of such a model is that it predicts that the eruption achieves the highest acceleration at a height comparable with the footpoint half-distance (Chen & Krall 2003; Vršnak 1990), which is fully consistent with observations (Chen et al. 2006; Vršnak et al. 1991).

However, in such a model, where the unstable structure is treated as an isolated system and no effects of resistive processes are considered, the accelerations are limited to values on the order of  $100 \text{ ms}^{-2}$ . Thus, such a model cannot explain the observed accelerations that can be as

high as several  $\text{km s}^{-2}$ . This is a direct consequence of the poloidal magnetic flux conservation, and the fact that the self-inductance increases with the size of the structure, i.e., the acceleration is limited due to the inductive weakening of the electric current (for details see Vršnak 2008).

The energy released in the flare/CME process is converted from the free energy stored in the non-potential coronal magnetic field, whereas the eruption itself is driven by the Lorentz force. This implies that there is electric current flowing through the eruptive structure. Most roughly, the intricate coronal current system might be approximated by a line-current loop anchored at both ends in the photosphere. In the absence of reconnection the magnetic flux encircled by the line-current and the photosphere is conserved. This flux can be expressed as  $\Phi = LI$ , where  $I$  is the electric current and  $L$  is the self-inductance of the system (Batygin & Toptygin 1962). Since the self-inductance is proportional to the circumference of the line-current (see, e.g., Jackson 1998, p. 218), the electric current must decrease as the size of the erupting structure increases, i.e.,  $I \propto \Lambda^{-1}$ , where  $\Lambda$  is the circumference of the current loop. Thus, the free energy,  $W = LI^2$ , decreases as approximately as  $W \propto \Lambda^{-1}$ , being converted into the kinetic and potential energy, and to the work done against the ‘‘aerodynamic’’ drag (Cargill 2004; Vršnak 2001). The Lorentz force decreases even more rapidly, since besides the electric current, the magnetic field decreases with height too. Thus, the acceleration decreases rapidly, meaning that the maximum CME speed is strongly limited. A similar behavior is found considering more realistic MHD representations based on flux-rope paradigm (Chen 1989; Démoulin & Aulanier 2010; Forbes 1990; Forbes & Priest 1995; Kliem & Török 2006; van Tend & Kuperus 1978; Vršnak 1990; Žic et al. 2007).

Thus, strong accelerations can be achieved only by removing the requirement of the poloidal flux conservation, i.e., by including the reconnection process that supplies the flux rope with additional poloidal flux (see, e.g., Anzer & Pneuman 1982; Steele & Priest 1989). In this respect it should be noted that in the series of papers (see references in, e.g., Chen et al. 2006), following the original idea from Chen (1989), it was proposed that the required flux supply of the order of  $d\Phi/dt \approx 10^{18} \text{ Mx s}^{-1}$  (adding up to  $\Phi \approx 10^{22} \text{ Mx}$  in total) is provided by the emerging flux. However, so strong flux emergence is not observed. On the other hand, the values of  $d\Phi/dt$  and  $\Phi$  measured in flares can be even considerably higher than required by the model (Forbes et al. 2006; Miklenic et al. 2009, 2007), i.e., reconnection is ample enough to be considered as the main source of the required poloidal flux. This led Chen & Kunkel (2010) to eventually adopt reconnection as the source of the poloidal flux in their model. Hereafter, we illustrate how magnetic reconnection affects the flux-rope eruption process.

### 3.2 The role of reconnection

When the effect of reconnection is included, the electric current does not decrease as  $I \propto \Lambda^{-1}$ , since it is affected by the

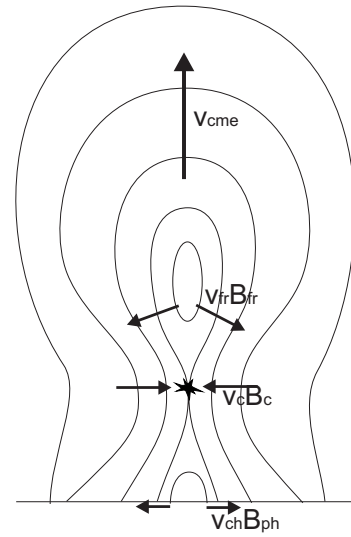


**Fig. 1** Effects of reconnection below the erupting flux rope, rising at a speed  $v_{\text{cme}}$ . The unit-length magnetic flux reconnects at the rate  $d\Phi/dt = v_c B_c$ , which roughly corresponds to the proxy  $v_{\text{ch}} B_{\text{ph}}$  as well as to the rate  $d\Phi_{\varphi}/dt = v_{\text{fr}} B_{\text{fr}}$  at which the flux-rope poloidal flux increases.

increase of the poloidal flux of the rope. Bearing in mind the relationship  $\Phi = IL$ , the current is now determined by  $I = (\Phi_0 + \Delta\Phi)/L$ , where  $\Phi_0$  is the initial flux, and  $\Delta\Phi$  is the flux added by reconnection  $\Delta\Phi = \int (d\Phi/dt) dt$ . In Figure 1 we present a 2D sketch of the erupting system that includes the reconnection below the rising flux rope (for a 3D analog of Figure 1 see Figure 8 of Schmieder et al. 2015). The rate at which the magnetic flux inflows into the diffusion region is determined by the convective electric field  $v_c B_c$ , i.e., the reconnected flux per unit length can be expressed as  $d\Phi/dt = v_c B_c$ . Bearing in mind the flux conservation, this also corresponds to the rate at which the unit-length flux is added to the flux rope (denoted as  $v_{\text{fr}} B_{\text{fr}}$  in Figure 1), i.e.,  $d\Phi/dt = d\Phi_{\varphi}/dt = v_{\text{fr}} B_{\text{fr}}$ , which forms a poloidal-flux shell around the rope and partly contributes to its expansion (for details see, e.g., Lin et al. 2005). Note that the reconnected flux also corresponds to the rate at which the magnetic flux accumulates in the flare-loop system below the diffusion region, as well as to the electric field induced in the current sheet. Furthermore, it should be approximately equal to the product of the velocity  $v_{\text{ch}}$  by which the chromospheric flare ribbons sweep over the photospheric magnetic field  $B_{\text{ph}}$ , i.e.,  $v_c B_c \approx v_{\text{ch}} B_{\text{ph}}$ , as proposed by Poletto & Kopp (1986), providing an estimate of how much of the magnetic flux is reconnected (see, e.g., Miklenic et al. 2009, 2007).

In the following, we consider a simple model presented in Sections 4.2. and 4.3 of Vršnak (2008), which is based on the model proposed by Vršnak (1990). Note that the model represents a kind of modified kink instability since the eruption is driven by the poloidal-field magnetic pressure gradient, enhanced by the already mentioned diamagnetic effect. In Figure 5b of Vršnak (2008) the flux-rope acceleration is presented as a function of the normalized height for dif-

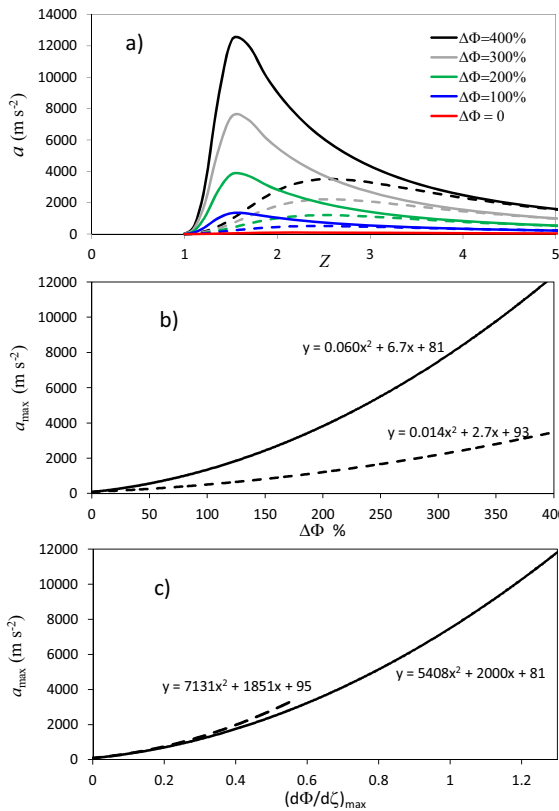


**Fig. 2** Dependence of the ejection acceleration on reconnection. a) The instantaneous acceleration,  $a$ , presented as a function of the normalized height,  $Z$ . Values of the total reconnected flux,  $\Delta\Phi$ , expressed in the percentage of the initial flux  $\Phi_0$ , are written in the inset. Full-line curves represent events where reconnection lasts during the period over which the eruption rises from  $Z = 1$  to  $Z = 2$ , whereas for the dashed-curve this range is  $1 < Z < 12$ . b) Dependence of the peak acceleration,  $a_{\max}$  on the total reconnected flux,  $\Delta\Phi$ . c) Dependence of the peak acceleration,  $a_{\max}$  on the peak reconnection rate,  $d\Phi/d\zeta$  (expressed in units of  $\Phi_0$ ).

ferent combinations of the flux-rope parameters in the absence of reconnection. The graph demonstrates that without reconnection the acceleration stays at values on the order of  $100 \text{ m s}^{-2}$ . Hereafter we illustrate the role of reconnection, i.e. we include the effect of increasing poloidal flux, to show that it provides accelerations up to  $10 \text{ km s}^{-2}$ . Let us note that a very similar outcome is obtained if the model is modified into a form where the torus instability initiates the eruption, i.e., where the gradient of the ambient field provides the driving force (see, e.g., Kliem & Török 2006; Török et al. 2010).

In Figure 2a we present the instantaneous acceleration  $a$  as a function of the normalized height  $Z$ , representing the ratio of the height and the half-distance between the flux-rope footpoints. In the absence of reconnection ( $\Delta\Phi = 0$ ; shown by red curve), the acceleration reaches only  $\sim 90 \text{ m s}^{-2}$ . In all other presented curves we let the poloidal flux inflow to start at  $Z = 1$ , i.e., soon after the eruption starts. To ease the numerical evaluation, the poloidal-flux increase rate is defined as a function of the geometrical parameter  $\zeta$ , related to

the normalized height as  $Z = (1 + \sin \zeta) / \cos \zeta$ . More specifically,  $d\Phi/d\zeta = k(1 - \cos(2\pi\zeta/\zeta_0))$ , where  $k$  regulates the amplitude of the reconnection rate and  $\zeta_0$  defines the flux-rope height up to which reconnection occurs (as already mentioned, it is taken that reconnection starts at  $Z = 1$ , i.e., at  $\zeta = 0$ ).

The graphs presented in Figure 2a illustrate two types of events; impulsive events (full-line curves) and more gradual ones (dashed-line curves). In the former class of events reconnection occurs during the flux-rope rise from  $Z = 1$  to  $Z = 2$ . In the latter class, the same amount of flux ( $\Delta\Phi = 100, 200, 300$ , and  $400\%$  of the initial flux  $\Phi_0$ ) is reconnected over the period corresponding to  $1 < Z < 12$ . The graph clearly shows that the acceleration is stronger for a larger total reconnected flux, and at the same value of  $\Delta\Phi$  it is stronger in more impulsive events. Furthermore, the acceleration peaks at larger heights in more gradual events. Note that at  $\Delta\Phi = 400\%$ , gained over the height range  $1 < Z < 2$ , the acceleration achieves a value of  $\sim 12 \text{ km s}^{-2}$ , which is sufficient to explain the most impulsively accelerated eruptions (e.g., Vršnak et al. 2007; Williams et al. 2005).

In Figure 2b the above noted dependence of the peak acceleration  $a_{\max}$  on the total reconnected flux  $\Delta\Phi$  is quantified. In the graph, an example of impulsive type of events ( $1 < Z < 2$ ; full line) is compared with a more gradual one ( $1 < Z < 12$ ; dashed line). Both curves show a quadratic-type of dependence, where the peak accelerations of the impulsive-reconnection events are considerably higher.

The dependence of  $a_{\max}$  on the maximum rate at which the poloidal flux increases,  $(d\Phi/d\zeta)_{\max}$ , is shown in Figure 2c. The presented two type of events are the same as those used in Figure 2b. The graph covers the range  $\Delta\Phi = 0 - 400\%$  for both types, clearly demonstrating that the impulsiveness of an event is a decisive factor that determines the peak acceleration. Namely, at the same value of  $(d\Phi/d\zeta)_{\max}$ , both the impulsive and gradual events show practically the same value of  $a_{\max}$ . Note that the graphs again show a quadratic-type of dependence.

On the other hand, the eruption peak velocity  $v_{\max}$  primarily depends on the total reconnected flux  $\Delta\Phi$ . Figure 3a, where the peak velocity  $v_{\max}$  is presented as a function of  $\Delta\Phi$ , reveals that at a given value of  $\Delta\Phi$  the impulsive ejections ( $1 < Z < 2$ , full line) and gradual ones ( $1 < Z < 12$ , dashed) achieve comparable peak velocities – although the impulsive events accelerate more rapidly, the acceleration time is shorter, so the two effects compensate each other and eventually, the final speed is similar to that of gradual events where weaker acceleration is compensated by longer acceleration time. On the other hand, Figure 3b shows that at a given value of  $(d\Phi/d\zeta)_{\max}$ , the peak velocity  $v_{\max}$  becomes significantly higher in gradual events, due to a considerably longer acceleration time, since the peak accelerations are comparable, as demonstrated by Figure 2c. Note that the dependence of  $v_{\max}$  on  $\Delta\Phi$  as well as on  $(d\Phi/d\zeta)_{\max}$  show a linear relationship. The outcome displayed in Fig-

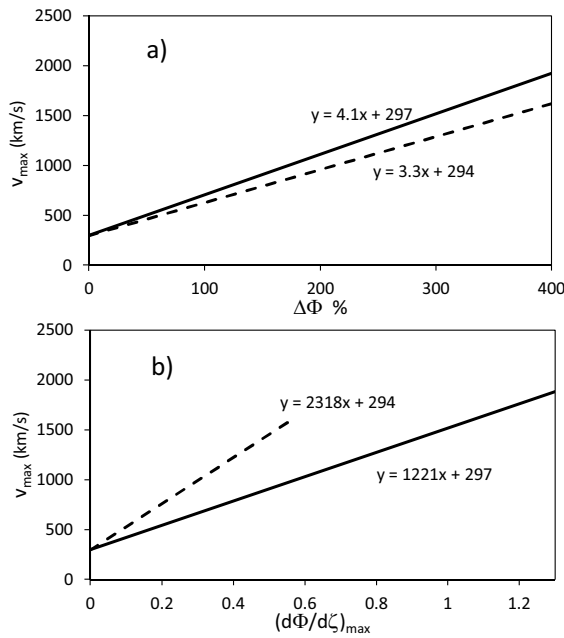


**Fig. 3** Dependence of the ejection peak velocity on: a) the total reconnected flux,  $\Delta\Phi$ ; b) the peak reconnection rate,  $(d\Phi/d\zeta)_{\max}$ . The case where reconnection lasts during the period over which the eruption rises from  $Z = 1$  to  $Z = 2$  is shown by full line, whereas for the dashed-curve this range is  $1 < Z < 12$ .

ure 3 explains the empirical results presented by Vršnak et al. (2005), Zhang & Dere (2006), Vršnak et al. (2007), and Bein et al. (2011).

To conclude, the peak acceleration is determined by the maximum reconnection rate, whereas the maximum speed is determined by the total reconnected flux. In other words, the eruption acceleration should be correlated with the flare impulsiveness, whereas the maximum speed of the eruption should be related to the total energy released by the associated flare. Both outcomes are consistent with the observational findings by Vršnak et al. (2005), Burkepille et al. (2004), Maričić et al. (2007), and Bein et al. (2012).

In Figure 4 the time evolution of the erupting system is illustrated by employing two examples characterized by  $\Delta\Phi = 400\%$ . The first one (shown by full-line curves) is an impulsive event, where reconnection takes place during the flux-rope rise from  $Z = 1$  to  $Z = 2$ , resulting in  $(d\Phi/d\zeta)_{\max} = 1.33\Phi_0$ . The second one is a more gradual event where the corresponding height range is  $1 < Z < 12$ , and is characterized by  $(d\Phi/d\zeta)_{\max} = 0.57\Phi_0$ .

In Figure 4a the instantaneous acceleration  $a$  (black) is shown together with the instantaneous reconnection rate  $d\Phi/d\zeta$  (gray) as a function of time. The graph clearly demonstrates synchronization of the acceleration and the reconnection rate. There is a small delay of the peak acceleration after the maximum reconnection rate. However, one should bear in mind that the effect of the aerodynamic drag is not taken into account. If it would be included in the calculation, it would result in a reduction of the acceleration with increasing speed, and would shift the accel-

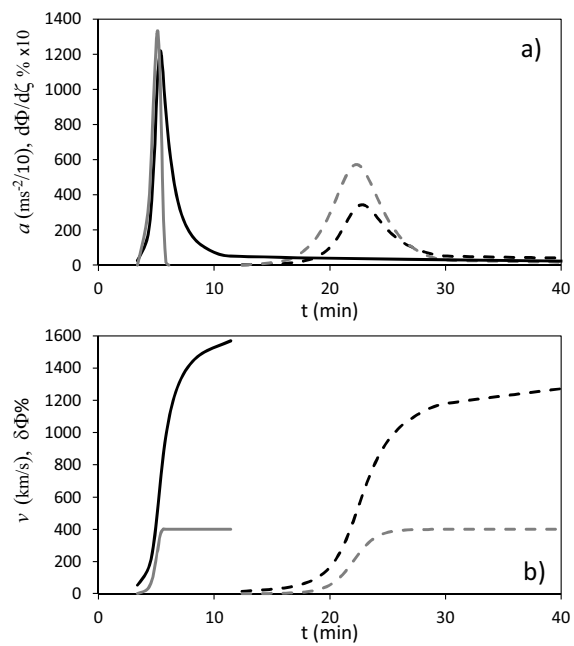


**Fig. 4** Synchronization of the ejection kinematics and the reconnection rate, i.e., the flare energy-release rate. a) Instantaneous acceleration,  $a$  (black; values are reduced by a factor of ten) and the instantaneous reconnection rate,  $d\Phi/d\zeta$  (gray; values are increased by a factor of ten), shown as a function of the ejection height,  $Z$ . b) Instantaneous ejection velocity,  $v$  (black) and the instantaneous reconnection rate,  $d\Phi/d\zeta$  (gray). In both graphs, the case  $\Delta\Phi = 400\%$  is presented, where reconnection starts at  $Z = 1$  and lasts until  $Z = 2$  (full lines) and until  $Z = 12$  (dashed).

eration curve to the left, i.e., the acceleration would peak earlier, which would reduce its delay with respect to the reconnection maximum. To conclude, the eruption acceleration should be closely synchronized with the flare impulsive phase (e.g., HXR and microwave burst, or derivative of the SXR flux), as found empirically by, e.g., Zhang et al. (2001), Vršnak et al. (2004), Zhang et al. (2004), Maričić et al. (2007), Temmer et al. (2010, 2008), and Bein et al. (2012).

In Figure 4b the instantaneous ejection velocity  $v$  (black) is shown together with the cumulative flux  $\delta\Phi$  reconnected until time  $t$  (gray), as a function of time. The graph clearly demonstrates synchronization of the velocity and the reconnected flux. To conclude, the rise of the eruption velocity should be closely synchronized with the flare SXR flux rise, as found empirically by, e.g., Zhang et al. (2001), Vršnak et al. (2004), and Zhang et al. (2004).

## 4 Discussion and Conclusions

In dynamical flares, causing the most powerful eruptive events originating in the solar atmosphere, there is a strong coupling between ideal MHD processes that initiate the eruption and the resistive processes responsible for the energy release in flares. A feedback relationship between the flare and the ejection is established through fast magnetic

reconnection that occurs in the current sheet formed below the erupting flux rope. Reconnection enhances significantly the acceleration of the ejection and on the other hand, provides a powerful energy release in the associated two-ribbon flare (see, e.g., Forbes 2000; Lin & Forbes 2000; Lin et al. 2004).

The energy released in the reconnection process is transported downwards to the chromosphere by electron beams and thermal conduction, forming there two bright ribbons aligned with the PIL. As reconnection proceeds, the flare ribbons, including HXR kernels (e.g., Temmer et al. 2007), expand away from the PIL, while the reconnected field lines form a growing X-ray flare loop system (e.g. Liu et al. 2004; Veronig et al. 2006; Vršnak et al. 2004).

The reconnection process below the erupting flux rope has also two important effects on the ejection itself. Firstly, the reconnection reduces the tension of the arcade field overlying the flux rope, which activates after the eruption onset (note that the overlying field is generally considered to be potential prior to the eruption, i.e., there is no tension until the field lines are being dragged by the eruption). Furthermore, reconnection increases the magnetic pressure below the flux-rope, which might play a significant role in the ejection dynamics (Anzer & Pneuman 1982; Forbes 1990; Lin 2004; van Tend & Kuperus 1978). Finally, the upward-directed reconnection jet brings the reconnected magnetic field to the flux-rope, providing it with additional poloidal flux. This strengthens the hoop force (Chen 1989) and prolongs and reinforces the flux-rope acceleration by reducing the effect of the inductive decay of the electric current (Vršnak 2008).

On the other hand, the expansion of the ejection determines the overall geometry of the system and the flows behind the flux-rope, which strongly affects the reconnection process (Vršnak & Skender 2005). The vortices behind the accelerating flux rope and evacuation of the space in the rear of the ejection are expected to enhance the reconnection process, which on the other hand, enhances the rope acceleration. In this way, the feedback between the flux-rope acceleration and the reconnection rate is established (Temmer et al. 2010; Vršnak 2008). The observed synchronization of the ejection acceleration and the flare energy release is a consequence of such a feedback, since the reconnection rate determines also the energy release in the flare (e.g., Asai et al. 2004; Miklenic et al. 2009; Temmer et al. 2007).

The described scenario is based on numerous empirical studies revealing various signatures of the flare/CME relationship. Certainly, the most important ones are various statistical studies of correlations between parameters of the flare energy release and the CME characteristics, the studies concerning the timing analysis that reveals synchronization of the flare energy release and the acceleration of the ejection, as well as various case studies showing tight morphological and evolutionary relationships between the two phenomena.

In this paper, it is shown by applying basic physical concepts that after some ideal instability initiates the eruption (e.g., kink or torus instability), intense magnetic reconnection below the erupting flux rope is needed to achieve the highest observed ejection accelerations and speeds. This means that a powerful ejection should inevitably cause also a powerful flare. In addition, more impulsively accelerated ejections should be accompanied by more impulsive flares. It is also shown that in the case of the most strongly accelerated ejections, where the observed accelerations attain values on the order of  $10 \text{ km s}^{-2}$ , the poloidal flux supplied to the flux rope during the eruption has to be several times larger than was the initial flux. Thus, in such events, a significant part of the flux rope has to be built during eruption itself. This also implies that it should be easier to achieve strong accelerations if the pre-eruptive structure contains a flux rope of a relatively small flux and is embedded in a large and strongly sheared magnetic arcade that will provide enough field for reconnection, i.e., to be able to supply the required poloidal flux to the rope. That would result in a strongly accelerated ejection and a powerful flare. The main physical reason is the fact that at large  $\Delta\Phi/\Phi_0$  the inductive decay of the current is strongly reduced, as shown at the beginning of Section 3.2. On the other hand, if the pre-eruptive rope contains a large flux  $\Phi_0$ , the current will decay relatively fast due to small  $\Delta\Phi/\Phi_0$ , which will prevent strong acceleration. However, the flare might still be powerful, since the total energy released depends directly on  $\Delta\Phi$ , i.e., by the time integral of the reconnecting flux. This straightforwardly explains the scatter in correlation between the flare intensity and CME speeds. Finally, it is shown that the reconnection impulsiveness (determining the impulsiveness of the flare energy release) regulates the peak acceleration, whereas the total reconnected flux (determining the total energy released in the flare) regulates the ejection speed.

*Acknowledgements.* This work has been fully supported by Croatian Science Foundation under the project 6212 "Solar and Stellar Variability".

## References

- Andrews, M. D. & Howard, R. A. 2001, *Space Sci. Rev.*, 95, 147
- Antiochos, S. K. 1998, *ApJ*, 502, L181
- Anzer, U. 1978, *Sol. Phys.*, 57, 111
- Anzer, U. & Pneuman, G. W. 1982, *Sol. Phys.*, 79, 129
- Asai, A., Yokoyama, T., Shimojo, M., et al. 2004, *ApJ*, 611, 557
- Aulanier, G. 2014, in *IAU Symposium*, Vol. 300, *IAU Symposium*, ed. B. Schmieder, J.-M. Malherbe, & S. T. Wu, 184–196
- Aurass, H., Vršnak, B., Hofmann, A., & Rudžjak, V. 1999, *Sol. Phys.*, 190, 267
- Batygin, V. V. & Toptygin, I. N. 1962, *Problems in Electrodynamics* (Academic Press, New York)
- Bein, B. M., Berkebile-Stoiser, S., Veronig, A. M., et al. 2011, *ApJ*, 738, 191
- Bein, B. M., Berkebile-Stoiser, S., Veronig, A. M., Temmer, M., & Vršnak, B. 2012, *ApJ*, 755, 44

- Berkebile-Stoiser, S., Veronig, A. M., Bein, B. M., & Temmer, M. 2012, *ApJ*, 753, 88
- Burkepile, J. T., Hundhausen, A. J., Stanger, A. L., St. Cyr, O. C., & Seiden, J. A. 2004, *J. Geophys. Res.*, 109
- Cargill, P. J. 2004, *Sol. Phys.*, 221, 135
- Carmichael, H. 1964, *NASA Special Publication*, 50, 451
- Chen, J. 1989, *ApJ*, 338, 453
- Chen, J. & Krall, J. 2003, *J. Geophys. Res.*, 108, 1410
- Chen, J. & Kunkel, V. 2010, *ApJ*, 717, 1105
- Chen, J., Marqué, C., Vourlidas, A., Krall, J., & Schuck, P. W. 2006, *ApJ*, 649, 452
- Démoulin, P. & Aulanier, G. 2010, *ApJ*, 718, 1388
- Dennis, B. R. & Zarro, D. M. 1993, *Sol. Phys.*, 146, 177
- Forbes, T. G. 1990, *J. Geophys. Res.*, 95, 11919
- Forbes, T. G. 2000, *J. Geophys. Res.*, 105, 23153
- Forbes, T. G., Linker, J. A., Chen, J., et al. 2006, *Space Sci. Rev.*, 123, 251
- Forbes, T. G. & Priest, E. R. 1995, *ApJ*, 446, 377
- Garren, D. A. & Chen, J. 1994, *Physics of Plasmas*, 1, 3425
- Gold, T. & Hoyle, F. 1960, *MNRAS*, 120, 89
- Gosling, J. T., Hildner, E., MacQueen, R. M., et al. 1976, *Sol. Phys.*, 48, 389
- Hirayama, T. 1974, *Sol. Phys.*, 34, 323
- Jackson, J. D. 1998, *Classical Electrodynamics*, 3rd Edition (Classical Electrodynamics, 3rd Edition, by John David Jackson, pp. 832. ISBN 0-471-30932-X. Wiley-VCH, July 1998.)
- Kahler, S. W., Moore, R. L., Kane, S. R., & Zirin, H. 1988, *ApJ*, 328, 824
- Kliem, B. & Török, T. 2006, *Physical Review Letters*, 96, 255002
- Kopp, R. A. & Pneuman, G. W. 1976, *Sol. Phys.*, 50, 85
- Kuperus, M. & Raadu, M. A. 1974, *A&A*, 31, 189
- Lin, J. 2004, *Sol. Phys.*, 219, 169
- Lin, J. & Forbes, T. G. 2000, *J. Geophys. Res.*, 105, 2375
- Lin, J., Ko, Y.-K., Sui, L., et al. 2005, *ApJ*, 622, 1251
- Lin, J., Raymond, J. C., & van Ballegooyen, A. A. 2004, *ApJ*, 602, 422
- Liu, W., Jiang, Y. W., Liu, S., & Petrosian, V. 2004, *ApJ*, 611, L53
- Low, B. C. & Zhang, M. 2002, *ApJ*, 564, L53
- MacQueen, R. M. & Fisher, R. R. 1983, *Sol. Phys.*, 89, 89
- Maričić, D., Vršnak, B., Stanger, A. L., & Veronig, A. 2004, *Sol. Phys.*, 225, 337
- Maričić, D., Vršnak, B., Stanger, A. L., et al. 2007, *Sol. Phys.*, 241, 99
- Miklenic, C. H., Veronig, A. M., & Vršnak, B. 2009, *A&A*, 499, 893
- Miklenic, C. H., Veronig, A. M., Vršnak, B., & Hanslmeier, A. 2007, *A&A*, 461, 697
- Moon, Y.-J., Choe, G. S., Wang, H., Park, Y. D., & Cheng, C. Z. 2003, *Journal of Korean Astronomical Society*, 36, 61
- Moon, Y.-J., Choe, G. S., Wang, H., et al. 2002, *ApJ*, 581, 694
- Moore, R. L., Sterling, A. C., Hudson, H. S., & Lemen, J. R. 2001, *ApJ*, 552, 833
- Mouschovias, T. C. & Poland, A. I. 1978, *ApJ*, 220, 675
- Neupert, W. M. 1968, *ApJ*, 153, L59
- Neupert, W. M., Thompson, B. J., Gurman, J. B., & Plunkett, S. P. 2001, *J. Geophys. Res.*, 106, 25215
- Pneuman, G. W. 1980, *A&A*, 81, 161
- Poletto, G. & Kopp, R. A. 1986, in *The lower atmosphere of solar flares*, p. 453 - 465, 453-465
- Priest, E. R. 1982, *Solar magneto-hydrodynamics* (D. Reidel Pub. Co., Dordrecht, Holland)
- Qiu, J., Wang, H., Cheng, C. Z., & Gary, D. E. 2004, *ApJ*, 604, 900
- Qiu, J. & Yurchyshyn, V. B. 2005, *ApJ*, 634, L121
- Ramsey, H. E. & Smith, S. F. 1966, *AJ*, 71, 197
- Sakurai, T. 1976, *PASJ*, 28, 177
- Schmieder, B., Aulanier, G., & Vršnak, B. 2015, *Sol. Phys.*
- Shanmugaraju, A., Moon, Y.-J., Dryer, M., & Umapathy, S. 2003, *Sol. Phys.*, 215, 185
- Sheeley, N. R., Walters, J. H., Wang, Y.-M., & Howard, R. A. 1999, *J. Geophys. Res.*, 104, 24739
- Steele, C. D. C. & Priest, E. R. 1989, *Sol. Phys.*, 119, 157
- Sturrock, P. A. 1966, *Nature*, 211, 695
- Švestka, Z. 1976, *Solar Flares* (Springer-Verlag, Berlin, Heidelberg)
- Švestka, Z. 1987, *Sol. Phys.*, 108, 411
- Švestka, Z. 2001, *Space Sci. Rev.*, 95, 135
- Temmer, M., Veronig, A. M., Kontar, E. P., Krucker, S., & Vršnak, B. 2010, *ApJ*, 712, 1410
- Temmer, M., Veronig, A. M., Vršnak, B., & Rybák, J., et al. 2008, *ApJ*, 673, L95
- Temmer, M., Veronig, A. M., Vršnak, B., & Miklenic, C. 2007, *ApJ*, 654, 665
- Titov, V. S. & Démoulin, P. 1999, *A&A*, 351, 707
- Török, T., Berger, M. A., & Kliem, B. 2010, *A&A*, 516, A49
- Török, T. & Kliem, B. 2003, *A&A*, 406, 1043
- van Tend, W. 1979, *Sol. Phys.*, 61, 89
- van Tend, W. & Kuperus, M. 1978, *Sol. Phys.*, 59, 115
- Veronig, A., Vršnak, B., Dennis, B. R., et al. 2002, *A&A*, 392, 699
- Veronig, A. M., Karlický, M., Vršnak, B., et al. 2006, *A&A*, 446, 675
- Vršnak, B. 1984, *Sol. Phys.*, 94, 289
- Vršnak, B. 1990, *Sol. Phys.*, 129, 295
- Vršnak, B. 2001, *Sol. Phys.*, 202, 173
- Vršnak, B. 2008, *Ann. Geophys.*, 26, 3089
- Vršnak, B., Klein, K.-L., Warmuth, A., Otruba, W., & Skender, M. 2003, *Sol. Phys.*, 214, 325
- Vršnak, B., Maričić, D., Stanger, A. L., & Veronig, A. 2004, *Sol. Phys.*, 225, 355
- Vršnak, B., Maričić, D., Stanger, A. L., et al. 2007, *Sol. Phys.*, 241, 85
- Vršnak, B., Ruždjak, V., Brajša, R., & Zloch, F. 1990, *Sol. Phys.*, 127, 119
- Vršnak, B., Ruzdjak, V., & Rempel, B. 1991, *Sol. Phys.*, 136, 151
- Vršnak, B. & Skender, M. 2005, *Sol. Phys.*, 226, 97
- Vršnak, B., Sudar, D., & Ruždjak, D. 2005, *A&A*, 435, 1149
- Vršnak, B., Temmer, M., Veronig, A., Karlický, M., & Lin, J. 2006, *Sol. Phys.*, 234, 273
- Wang, H., Qiu, J., Jing, J., & Zhang, H. 2003, *ApJ*, 593, 564
- Williams, D. R., Török, T., Démoulin, P., van Driel-Gesztelyi, L., & Kliem, B. 2005, *ApJ*, 628, L163
- Yashiro, S., Gopalswamy, N., Michalek, G., et al. 2004, *J. Geophys. Res.*, 109, A07105
- Zhang, J. & Dere, K. P. 2006, *ApJ*, 649, 1100
- Zhang, J., Dere, K. P., Howard, R. A., Kundu, M. R., & White, S. M. 2001, *ApJ*, 559, 452
- Zhang, J., Dere, K. P., Howard, R. A., & Vourlidas, A. 2004, *ApJ*, 604, 420
- Žic, T., Vršnak, B., & Skender, M. 2007, *J. Plasma Phys.*, 73, 741